Electronic supplementary information

Electrophoretic assisted Fabrication of Additive-free WS_2 Nanosheet Anodes for High Energy Density Lithium-Ion Batteries

*Xuan-Manh Pham,‡ Niraj Nitish Patil,‡ Syed Abdul Ahad, Nilotpal Kapuria, Kwadwo Asare Owusu, Hugh Geaney, Shalini Singh, Kevin M. Ryan**

Department of Chemical Sciences and Bernal Institute, University of Limerick, Limerick, V94 T9PX, Ireland

E-mail: Kevin.M.Ryan@ul.ie

‡ Xuan-Manh Pham and Niraj Nitish Patil have contributed equally to this work.

Experimental section

Materials

Tungsten hexacarbonyl ($W(CO)_6$, 97%), oleylamine (OLA, 70%), squalane (96%), oleic acid (OA, 90%), phenyl disulphide (99%), and trioctylphosphine (TOP, 97%) were purchased from Sigma Aldrich. Toluene, ethanol, hexane, and isopropanol (IPA) were bought from Lennox, Ireland. Tetradecyl phosphonic acid (TDPA) was purchased from Plasmachem. All reagents were used as received without further purification. Cu foil (9 μm thick) was provided by Pi-Kem. Battery-grade 1.0 M $LiPF_6$ in ethylene carbonate (EC) and diethyl carbonate (DEC), EC-DEC (1:1 v/v) and vinylene carbonate (VC, 97 %, additives) were purchased from Sigma Aldrich.

Synthesis

Two different WS_2 NSs were prepared, with control over crystal phase and particle morphology, using a colloidal hot injection setup described in our recent work.[1] Firstly,

semiconducting WS_2 NSs (denoted NS-2H) were synthesized by adding oleylamine, OLA (7 mL) into a 25 mL three-neck flask. The solution was evacuated at 120°C for 30 minutes to remove all moisture and oxygen. At the same time, W stock solution ($W(CO)_6$ (0.25 mmol), oleic acid (2 mL) and 10 mol% of tetradecyl phosphonic acid (TDPA)) and S stock solution (1 mmol of S in 5 mL of oleylamine, OLA) were prepared separately inside the glovebox under vigorously stirred at 130 °C until $W(CO)_6$ and S completely dissolved in solution, then both solutions were mixed in an oxygen and moisture-free atmosphere at 130 °C. Afterwards, the reaction vessel was heated to 320 °C under an Ar atmosphere, at which point a mixture of W stock solution and S stock solution was injected into the flask at a rate of ~0.7 ml min^{-1}. The reaction mixture was kept at 320 °C for 2 h. The NSs were washed twice with a mixture of 10 ml toluene and 10 ml ethanol the first time and a mixture of 5 ml hexane and 5 ml IPA the second time at 5,000 rpm for 5 min. The supernatants were discarded and the NSs were collected and redispersed into 5 mL hexane for further experiments. For metallic NS synthesis (denoted NS-1T'), the above procedure was replicated but squalene was substituted for OLA (2 mL) in the preparation of S stock solution, WCl_6 replaced $W(CO)_6$ in the preparation of W stock solution, and OA was added initially into a 25 mL three-neck flask instead of OLA.

Electrophoretic Deposition. The deposition solution was prepared by diluting 0.4 mL of the as-synthesized NSs in hexane solution with 10 mL hexane. Two Cu foil plates held approximately 2 cm apart were immersed in the bath, and a direct current (DC) voltage of 300 V was applied using a high-voltage power supply (TECHNIX SR-5-F-300). Deposition of NSs occurred on the positive electrode, and the thickness of the resulting film could be controlled by varying the concentration and total immersion time. All battery electrodes achieved a mass loading of 0.4–0.5 mg/cm^2.

Ligand Removal. The resultant films typically included long-chain organic ligands (OLA and OA, TDPA) which are low conductivity. Removal of these ligands not only enhances film

conductivity but also reduces inactive material.[2, 3] The electrodes underwent this treatment by being submerged in a 20 mM solution of ammonium sulfide in methanol for 30 s, followed by a methanol rinse to remove any residual ammonium sulfide and any free organics. Afterwards, the electrodes were dried for 12 h at 70 °C before the cell assembly.

Material characterisation

Transmission electron microscopy (TEM) and dark–field scanning transmission electron microscopy (DF–STEM) were obtained on a JEOL JEM–2100F field emission microscope at an acceleration voltage of 200 kV, equipped with a Gatan Ultra Scan CCD camera and an EDAX Genesis energy dispersive X–ray spectroscopy (EDS) detector. Raman spectroscopy was carried out with a Horiba Labraman 300 spectrometer system equipped with a 532 nm laser. UV–Vis–NIR spectroscopy was performed on a Cary 5000 spectrophotometer in 1 cm path length cuvettes using toluene as solvent. X–ray photoelectron spectroscopy (XPS) was collectetd on a Kratos AXIS ULTRA spectrometer using a mono Al Kα X–ray gun.

Electrochemical characterization

Half-cells (CR 2032) were assembled in an argon filled glove box (Vigor) containing an active electrode, Li metal foil as a counter electrode, and a polypropylene separator (Celgard 2400) soaked in electrolyte. The electrolyte solution was 1 M $LiPF_6$ (EC:DEC, 50:50 v/v) + 3% VC (Sigma Aldrich). Galvanostatic cycling tests were carried out using a Neware battery cycler instrument in a potential range of 0.01–3.0 V. All current densities were calculated based on the mass of the active material. Electrochemical impedance spectroscopy (EIS) was performed in a frequency range of 0.1 Hz to 10 kHz, and cyclic voltammetry (CV) was performed using a scan rate of 0.05 mV s^{-1}.

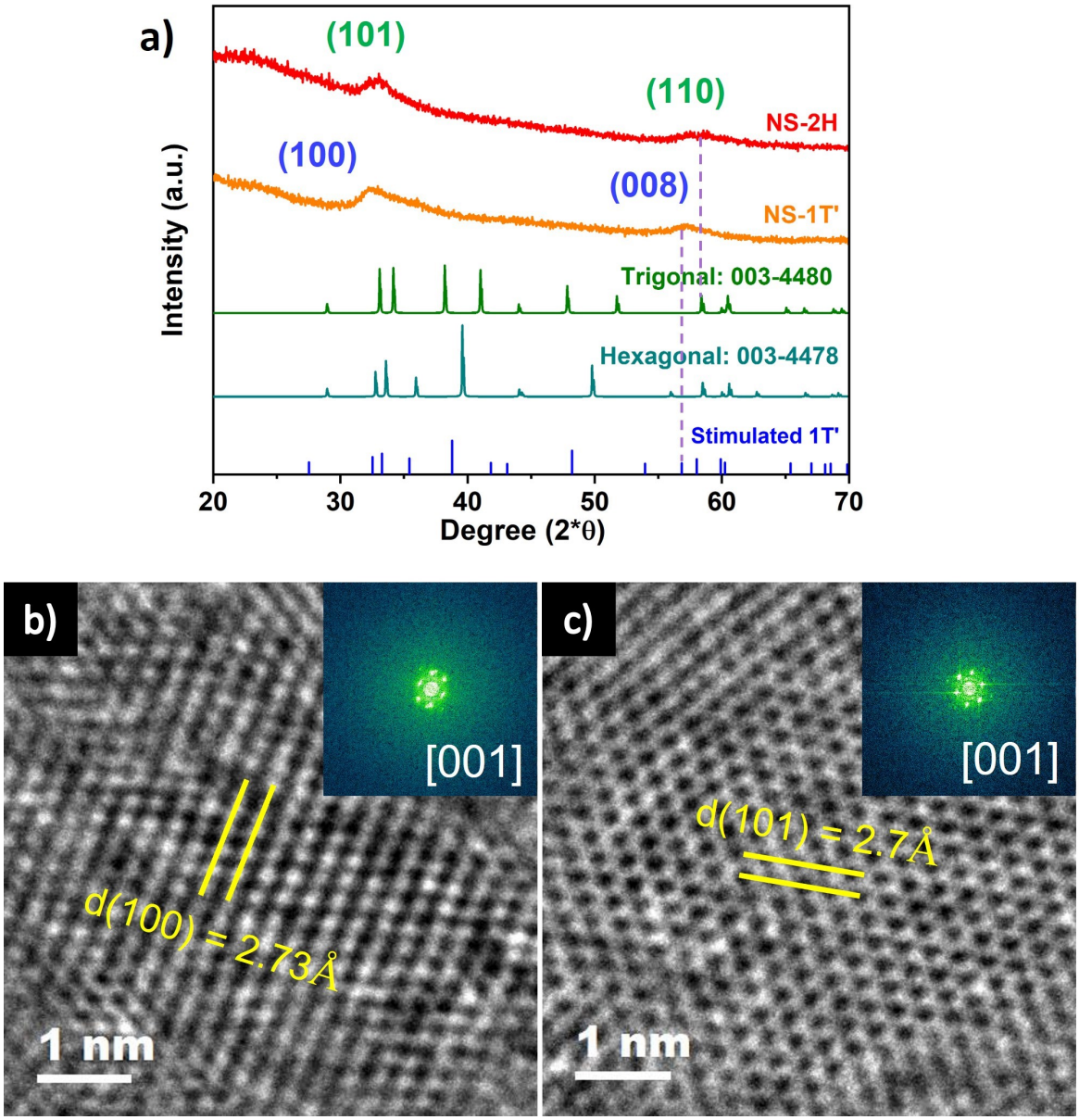

Fig. S1 a) XRD pattern of NS-1T' and NS-2H. HR-TEM images of b) NS-1T' with FFT inset and c) NS-2H with FFT inset.

The XRD analysis confirmed the presence of 1T' phase and 2H phase in NS-1T' and NS-2H samples, respectively. The XRD pattern of NS-2H (red) matched with standard pattern (003-4480) with peaks at ~33.0° and 58.3° characteristic of trigonal structure (2H phase), assigned to (101) and (110) planes, respectively. The XRD pattern of NS-1T' occurred two peaks at ~32.5° and 57.1°, matched with hexagonal standard pattern (003-4478) and stimulated 1T' pattern.

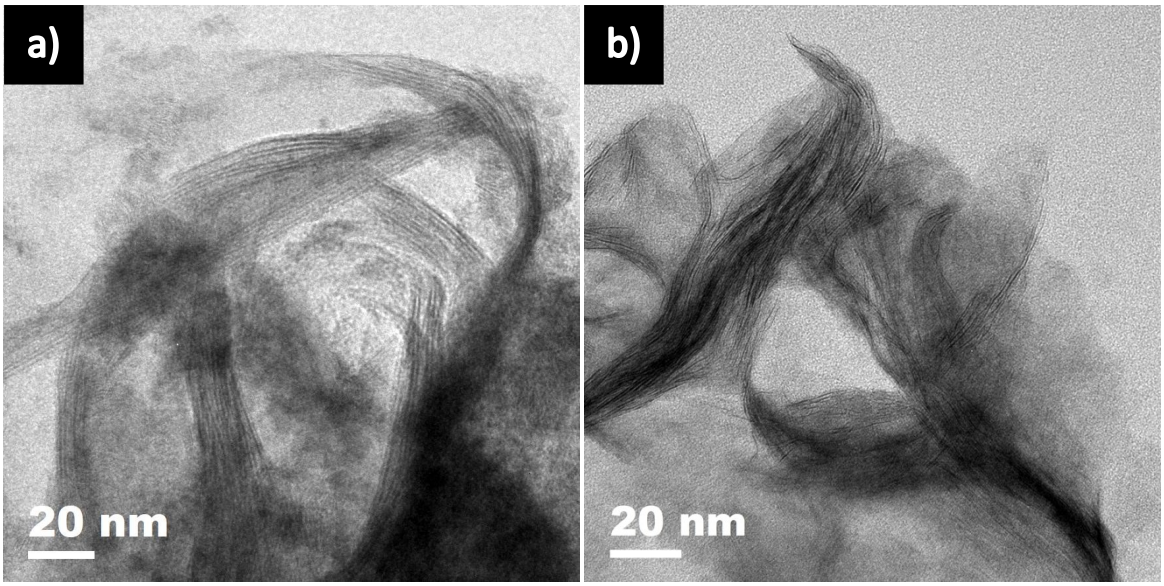

Fig. S2 HR-TEM images of a) NS-1T' and b) NS-2H.

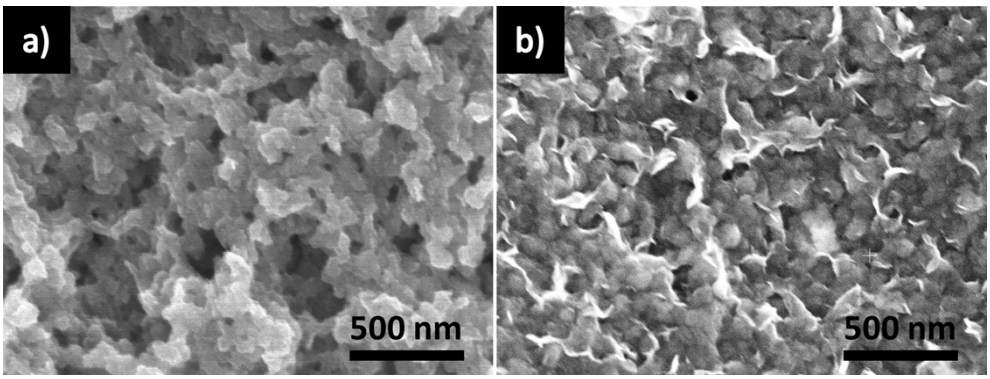

Fig. S3 HR-SEM images of a) NS-1T' and b) NS-2H deposited by EPD.

NS-1T' (Fig. S3a) and NS-2H (Fig. S3b) were deposited uniformly by EPD on copper foils. Nanosheets (NSs) were arranged randomly, creating space sites that enable electrolytes to immerse easily into the electrodes. This facilitates the Li^+ diffusion and improves the electrical conductivity.

Table S1 Comprehensive comparison table for WS_2 as anode material.

Anode Material	Capacity retention (mA h g^{-1})	No. of Cycles	Current Density (mA g^{-1})	Rate Performance Capacity @ Current Density (mA h g^{-1}@mA g^{-1})	References
WS_2 NS-2H	579	600	~86.6	652 @ 43.3 511 @ 433 411 @ 866 272 @ 2165	This work
WS_2@HNCSs	631.6	150	~500	801.4 @ 100 545.6 @ 2000	ACS Appl. Mater. Interfaces 2016, 8, 29, 18841–18848.[4]
2H-WS_2	~275	100	800	457 @ 100 438 @ 200 421 @ 300 295 @ 800	Nano Lett. 2018, 18, 11, 7155–7164.[5]
WS_2/carbon nanofibers (WS_2/CNFs)	458	100	1000	770 @ 100 635 @ 200 554 @ 500 495 @1000	Sci. Bull. 2016, 61, 3, 227–235.[6]
WS_2@$TiNb_2O_7$ HNs	627	200	1000	660 @ 200 632 @ 500 578 @ 2000 527 @ 4000	Chem. Eng. J., 2020, 382, 122800.[7]
WS_2–PCBM/MWCNT	485.73	500	1000	816.60 @ 200 539.94 @ 500 343.68 @ 1000 187.88 @ 2000	Energy Fuels, 2023, 37, 20, 16105–16118.[8]
WS_2/graphene nanosheets (WS_2/GNSs)	705	200	250	-	Tungsten, 2024, 6, 124–133.[9]
WS_2 NS	242	600	433	615.02 @ 108 550.82 @ 216 450.27 @ 433 336.84 @ 866	Energy Technol. 2022, 10, 2200117.[10]
C@WS_2@Gs	356.5	150	100	587.1 @ 200 535.6 @ 500 415.5 @ 1000 217.8 @ 2000	Chem. Eng. J., 2019, 375, 122033.[11]
WS_2/graphene/carbon nanofiber (WS_2/GCNF)	1128.2	100	100	-	Nanoscale, 2016, 8, 16387-16394.[12]
Hexagonal WS_2 nanosheets ((750 °C)	241	20	433	350 @ 866 250 @ 2165	New J. Chem., 2020, 44, 1594-1608.[13]
Plate-like WS_2	~380	200	~108	486 @ 54 449.6 @ 216 390.7 @ 433 334.7 @ 866	ChemistrySelect 2020, 5, 14183 – 14189.[14]

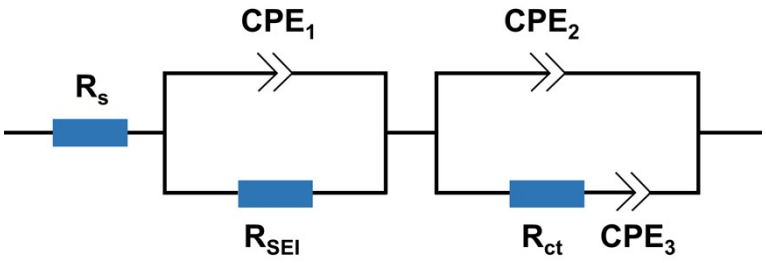

Fig. S4 An equivalent circuit used for fitting of EIS data.

The equivalent circuit contains R_s which is the resistance of electrolyte. R_{SEI} stands for the resistance of the SEI layer. R_{ct} is associated with the charge transfer resistance. CPE_1, CPE_2, and CPE_3 are the capacitance (constant phase element of SEI layer, the electrode/electrolyte interface).

Table S2 Tabulation of R_s, R_{SEI} and R_{ct} value of NS-1T' and NS-2H at different cycle no. cycled.

Electrode	NS-1T'			NS-2H		
Cycle	R_s (Ω)	R_{SEI} (Ω)	R_{ct} (Ω)	R_s (Ω)	R_{SEI} (Ω)	R_{ct} (Ω)
1st	99.92	37.87	2317	26.2	30.2	1110
10th	73.88	39.43	1764	28.97	30.74	899.2
100th	60.93	41.48	1490	17.77	32.66	701.2

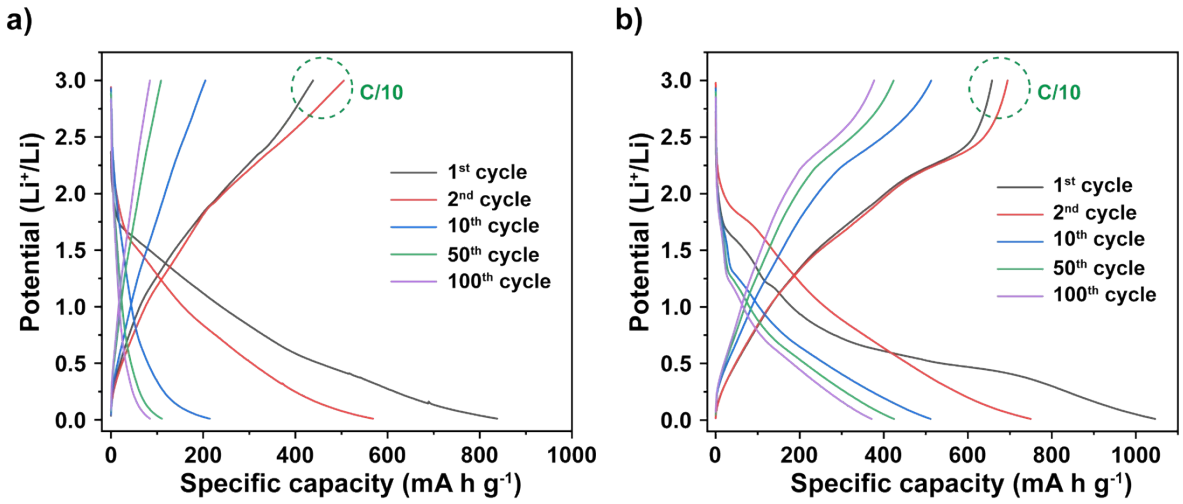

Fig. S5 Charge-discharge profiles of a) NS-1T' and b) NS-2H cycled at a rate of C/10 for the first 5 cycles and 1C thereafter.

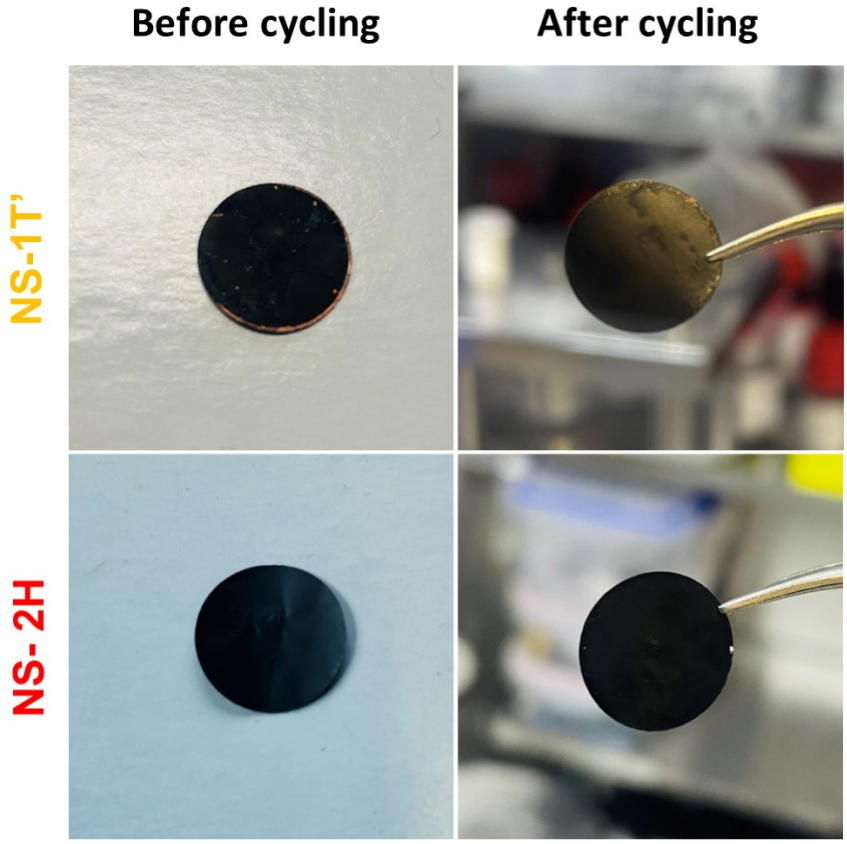

Fig. S6 Optical images of NS-1T' and NS-2H electrodes before and after cycling 100 cycles.

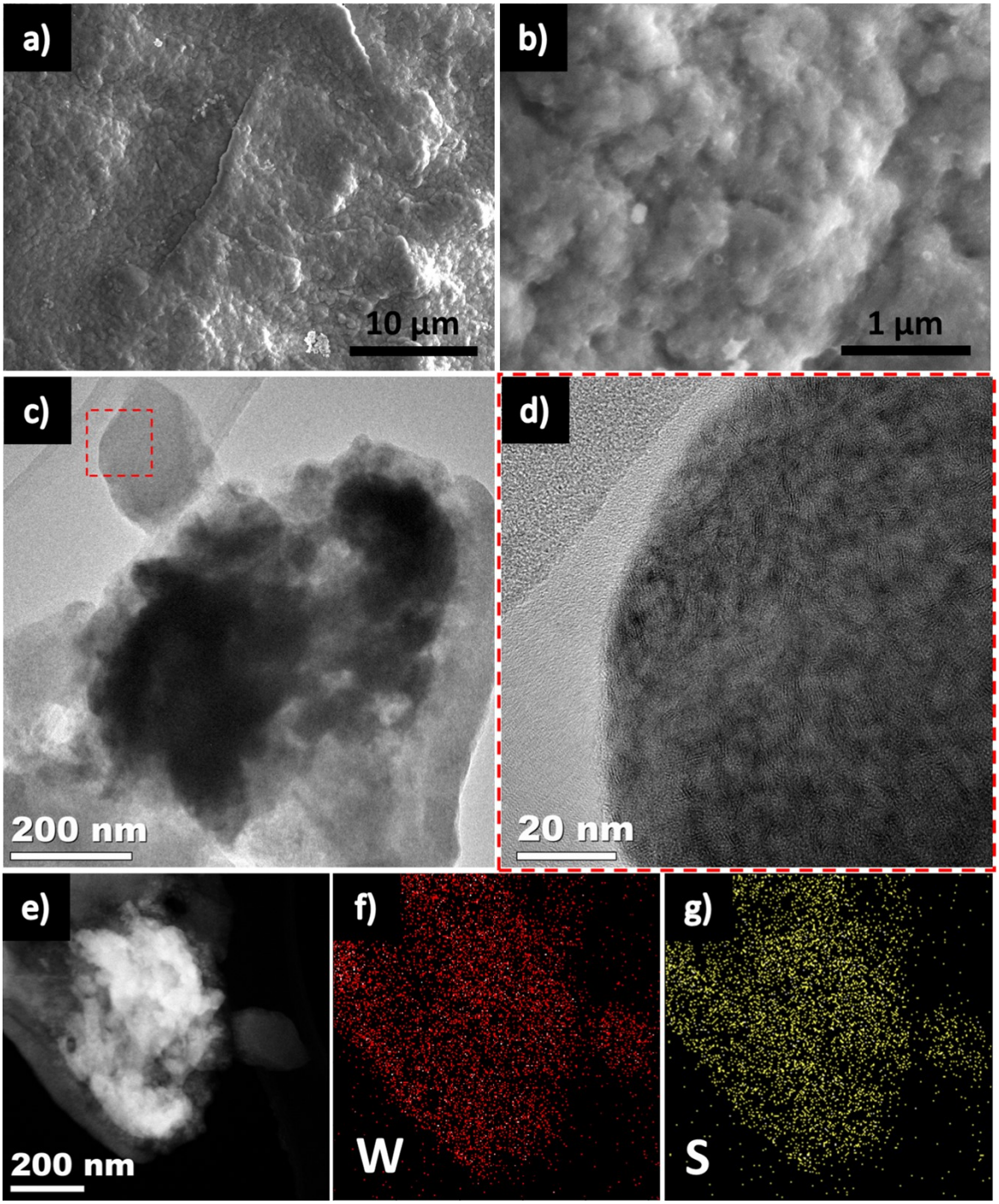

Fig. S7 Post mortem of the NS-1T' after 100 cycles: (a and b) SEM images, (c and d) TEM images, e) STEM and (f and g) elemental mapping of W and S of NS-1T', respectively.

Further post-mortem HRTEM analysis:

2H phase WS_2 after 100 cycling:

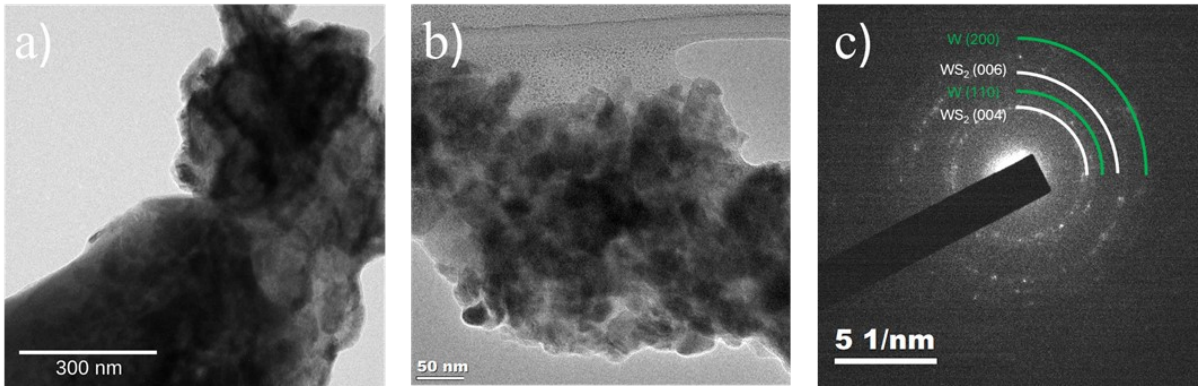

Fig. S8 a) and b) Low and high-resolution TEM images of NS-2H after 100 cycles. c) SAED pattern of NS-2H after 100 cycles, indicating the presence of crystalline WS_2 along with W nanoparticles.

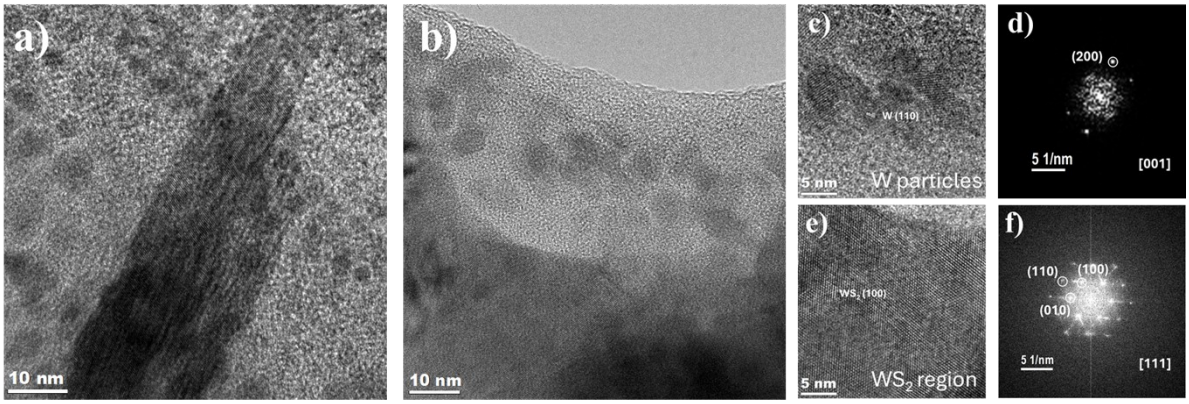

Fig. S9 a) and b) High-resolution TEM images of NS-2H after 100 cycles, showing the presence of both crystalline WS_2 nanosheets and W nanoparticles. c) and d) High-resolution TEM images of the region from figure b), highlighting W nanoparticles, with FFT confirming the crystalline structure of W. e) and f) High-resolution TEM images of the region from figure b), focusing on WS_2 nanosheets, with FFT corresponding to the WS_2 crystal structure.

1T' phase WS2 after 100 cycling:

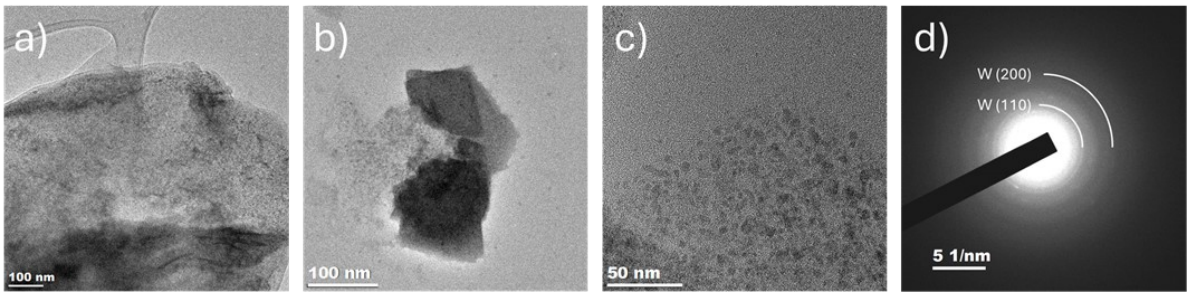

Fig. S10 a) and b) Low-resolution TEM images of NS-1T' after 100 cycles, showing that most of the WS_2 has converted into an amorphous phase. c) High-resolution TEM image of NS-1T' after 100 cycles, showing the presence of W nanoparticles. d) SAED pattern of NS-1T' after 100 cycles, indicating the presence of amorphous WS_2 along with W nanoparticles.

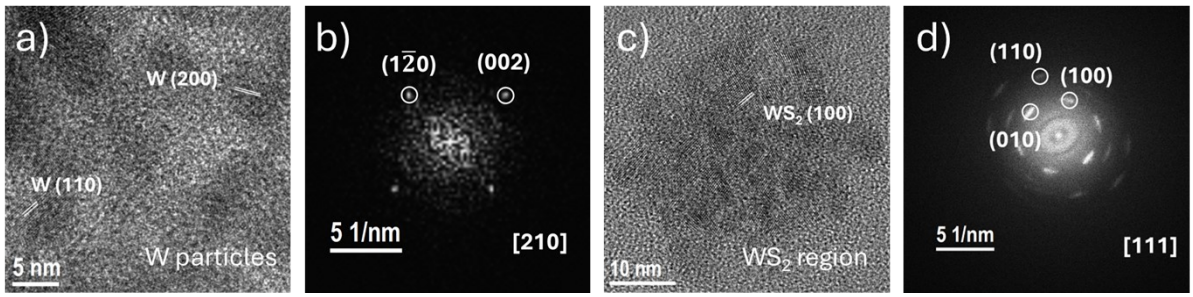

Fig. S11 a) and b) High-resolution TEM images of W nanoparticles, with FFT analysis confirming the crystalline structure of W. c) and d) High-resolution TEM images of WS_2 nanosheets, showing fragmentation, with FFT corresponding to the WS_2 crystal structure.

References

1. N. Kapuria, N. N. Patil, A. Sankaran, F. Laffir, H. Geaney, E. Magner, M. Scanlon, K. M. Ryan and S. Singh, *J. Mater. Chem. A*, 2023, **11**, 11341-11353.
2. H. Zhang, B.-R. Hyun, F. W. Wise and R. D. Robinson, *Nano Lett.*, 2012, **12**, 5856-5860.
3. D.-H. Ha, T. Ly, J. M. Caron, H. Zhang, K. E. Fritz and R. D. Robinson, *ACS Appl. Mater. Interfaces*, 2015, **7**, 25053-25060.
4. X. Zeng, Z. Ding, C. Ma, L. Wu, J. Liu, L. Chen, D. G. Ivey and W. Wei, *ACS Appl. Mater. Interfaces*, 2016, **8**, 18841-18848.
5. S. Bellani, F. Wang, G. Longoni, L. Najafi, R. Oropesa-Nuñez, A. E. Del Rio Castillo, M. Prato, X. Zhuang, V. Pellegrini, X. Feng and F. Bonaccorso, *Nano Lett.*, 2018, **18**, 7155-7164.
6. S. Zhou, J. Chen, L. Gan, Q. Zhang, Z. Zheng, H. Li and T. Zhai, *Sci. Bull.*, 2016, **61**, 227-235.
7. L. Yin, D. Pham-Cong, I. Jeon, J.-P. Kim, J. Cho, S.-Y. Jeong, H. Woo Lee and C.-R. Cho, *Chem. Eng. J.*, 2020, **382**, 122800.
8. B. Mondal, A. Azam and S. Ahmad, *Energy & Fuels*, 2023, **37**, 16105-16118.
9. Y.-L. Wu, J.-B. Hong, W.-X. Zhong, C.-X. Wang, Z.-F. Li and S. Dmytro, *Tungsten*, 2024, **6**, 124-133.
10. S. Sengupta and M. Kundu, *Energy Technology*, 2022, **10**, 2200117.
11. I. Kim, S.-W. Park and D.-W. Kim, *Chem. Eng. J.*, 2019, **375**, 122033.
12. L. Zhang, W. Fan and T. Liu, *Nanoscale*, 2016, **8**, 16387-16394.
13. P. Sharma, A. Kumar, S. Bankuru, J. Chakraborty and S. Puravankara, *New J. Chem.*, 2020, **44**, 1594-1608.
14. S. Sengupta and M. Kundu, *ChemistrySelect*, 2020, **5**, 14183-14189.